4
Cleaning of Absorber Pore

It is revealed in Chapter 3 that dust deposition poses a major challenge towards the operation of an open volumetric air receiver. Therefore, a need of cleaning device arises for mitigating the effect of dust deposition and sustainable operation. There are a number of dust collectors, which can be used for the system. These are compared in Table 4.1. In view of the operation and accessibility at high altitude, maintenance and safety of the system, finally, a cyclone separator is selected [Singh, 2014]. Cyclone separators are the most widely used devices to separate dust, particulate matter and other solid and liquid particles from air [Wang, 2004]. Cyclone separator is made of cylindrical barrel and a conical section. The designed cyclone separator is shown in Figure 4.1. This Figure shows that the length of barrel and conical section is 2 times the cyclone separator diameter. This is termed as a 2D2D design. In a cyclone separator, air moves in a helical path leading to the formation of vortices. On the account of interaction between gravity, centrifugal, drag and buoyant forces, the dust particles separate from air near the wall of the separator. The heavier particles separate, mostly, in the cylindrical barrel and lighter particles separate at the conical section. The clean air reverses its path and sucked out of the separator using a suction device. Thus, dimensions of barrel and conical section are to be carefully selected, which are based on cyclone diameter.

Table 4.1: Comparison between different dust collection/cleaning systems.

S.No.	Dust Collector/Cleaner	Advantages	Disadvantages
1.	Electrostatic Precipitator	1. High collection efficiency 2. Can work at high temperature	1. High electricity requirements 2. Maintenance is difficult at high altitude 3. May catch fire due to sparks during collection of particles
2.	Bag filter	1. Cheap 2. Easy to install	1. Cannot work at high temperature 2. Regular cleaning is required
3.	Cyclone separator	1. Low initial and running cost 2. No moving parts so nearly maintenance free. 3. Can be used at high temperatures	1. Very small particles (diameter< 1µm) are difficult to separate. 2. High power requirement if pressure-drop is high.

The selected cyclone separator diameter (e.g. D_c = 50 mm) for the presented experiment is based on the operating mass flow rate of 4-6 g/s and the required area-averaged air-speed of about 12-15 m/s at the inlet of the cyclone separator at the room temperature of 30 °C. This is the expected air mass flow rate through the porous absorber, which was designed for the experimental evaluation of the open volumetric air receiver [Sharma *et al.*, 2015a,b].

Component of cyclone separator	Dimension (mm)	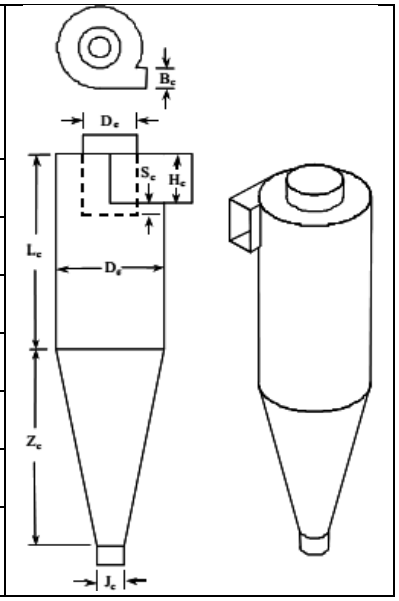
Cyclone diameter (D_c)	50	
Barrel length (L_{cs})	100	
Cone length (Z_c)	100	
Cyclone Outlet diameter (D_e)	25	
Inlet height (H_c)	25	
Inlet width (B_c)	12.5	
Outlet pipe length (H_c+S_c)	31.25	

Figure 4.1: Designed cyclone separator with dimensions; source of representative diagram: [Wang, 2004].

Collection efficiency of a cyclone separator increases with the number of helical turns (N_e), which is as follows [Lapple, 1951]:

$$N_e = \frac{1}{H_c}\left[L_{cs} + \frac{Z_c}{2}\right] \quad . \tag{4.1}$$

The cut point diameter, which is a measure of size of dust particle that can be collected in the cyclone separator, is given by Lapple (1951):

$$d_{pc} = \left[\frac{9\mu B_c}{2\pi N_e V_i(\rho_p - \rho_g)}\right]. \tag{4.2}$$

The collection efficiency of a cyclone separator is measure of the ratio of collected to injected dust at a given size. It depends on the number of turns, the inlet velocity, the inlet width, the properties of gas and the density of dust particles. For example, Shepherd and Lapple (1939) presented a model for collection efficiency as follows:

$$\eta_j = \frac{1}{\left[1 + \left(d_{pc}/d_{pj}\right)^2\right]} \quad . \tag{4.3}$$

Thus, if a cyclone separator is designed with a cut point diameter, say, ≤ 10 μm then the collection efficiency of this system will be higher for the larger particle size. The selected geometrical parameters of an experimental cyclone separator, as shown in Figure 4.1, ensures the targeted collection efficiency of greater than 95% for a particle size less than 50 μm. This is experimentally verified by Singh (2014) with the given flow conditions.

4.1 PARTICLE MOTION IN A CYCLONE SEPARATOR

As explained, the separation of dust particles depends on the acting forces. The force balance provides particle size distribution for a given flow condition. The dust laden air enters tangentially in the designed cyclone separator with a velocity denoted by V_i. Let us consider a particle moving in a trajectory of radius r_p with the tangential velocity denoted by V_t and the radial velocity by V_r. This particle experiences several types of forces, such as, the centrifugal

force (F_c), the drag force (F_d) and the buoyancy force (F_b). These are shown in Figure 4.2. Following aspects are assumed for the force balance for a given flow condition:

a) the particle has a spherical geometry, and
b) the particle moves in the circular path with no appreciable movement along the vertical direction.

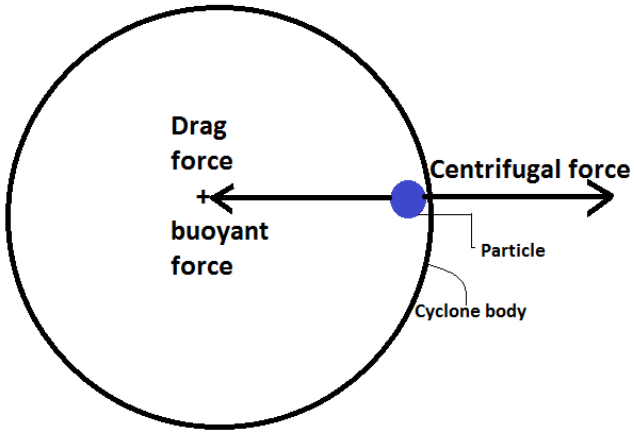

Figure 4.2: Forces acting on a particle in circular path.

The centrifugal force acts radially outwards and is given as

$$F_c = \frac{4}{3}\pi\rho_p r_p^3 \frac{V_t^2}{r_p}. \tag{4.4}$$

The drag force on a particle as given by Stokes law is

$$F_d = -6\pi\mu r_p V_r \ . \tag{4.5}$$

The negative sign shows that the nature of force is against the motion of particle. Because of the volume of displaced fluid surrounding a particle the buoyant force acts radial inward and is opposite to the centrifugal force. This is calculated as follows:

$$F_b = -\frac{4}{3}\pi\rho_f r_p^3 \frac{V_t^2}{r}. \tag{4.6}$$

Further, according to the Newton's second law of motion and assuming that the particle has reached the terminal velocity results in,

$$0 = -6\pi\mu r_p V_r - \frac{4}{3}\pi\rho_f r_p^3 \frac{V_t^2}{r} + \frac{4}{3}\pi\rho_p r_p^3 \frac{V_t^2}{r}. \tag{4.7}$$

On solving for r_p we obtain

$$r_{ps} = 3\sqrt{\left(\frac{\mu V_r r}{2V_t^2(\rho_p - \rho_f)}\right)}. \tag{4.8}$$

Stokes law is used in this force balance, which is valid for the flow having Reynolds number ~ 1 [White, 2011]. Such a flow is called creeping flow. However, in a cyclone separator the velocity and Reynolds number are generally high (>>1) and hence Stokes law is inadequate. Therefore, the formulation of drag force on a spherical particle is used for the force balance, which is as follows:

$$\text{Drag force} = \frac{1}{2} C_d \rho A V_r^2 \ . \tag{4.9}$$

Using eq. (4.7) we can write

$$0 = -\frac{1}{2}C_d\rho A V_r^2 - \frac{4}{3}\pi\rho_f r_p^3 \frac{V_t^2}{r} + \frac{4}{3}\pi\rho_p r_p^3 \frac{V_t^2}{r}\,. \tag{4.10}$$

On solving for r_p we get

$$r_{pd} = \frac{3rC_d\rho_f V_r^2}{8V_t^2(\rho_p - \rho_f)}, \tag{4.11}$$

where, C_d = Drag coefficient ~ 0.5 for smooth sphere [White, 2011] and A= Projected area of particle (πr^2 for sphere) normal to the mean flow direction. The eqs. (4.11) and (4.8) depict the particle size distribution on a given circular trajectory.

4.2 PRESSURE-DROP IN A CYCLONE SEPARATOR

The required power for a cyclone separator would decide if this system can be operated at all time or only during a limited period in an emergency condition. This is estimated from the pressure-drop across inlet and outlet (suction side) of a cyclone separator. Table 4.2 presents some of the well-known correlations for estimating the pressure-drop in the 2D2D configurations.

Table 4.2: Different models for pressure-drop estimation in cyclone separator.

Model	Pressure-drop	Involved parameters
Shepherd and Lapple, (1939)	$\Delta p = \frac{1}{2}\rho_g V_i^2 H_v$	$H_v = K\left(\frac{H_c B_c}{D_e^2}\right), K = 16$
Casel and Martinez, (1983)	$\Delta p = \frac{1}{2}\varsigma_c \rho_g V_i^2$	$\varsigma_c = 3.33 + 11.3(H_c B_c / D_e^2)^2$
Coker, (1993)	$\Delta p = \frac{1}{2}\rho_g V_i^2 H_v$	$H_v = K\left(\frac{H_c B_c}{D_e^2}\right), K = 9.47$
Dirgo and Leith, (1985)	$\Delta p = \frac{1}{2}\rho_g V_i^2 H_v$	$H_v = 20\left(\frac{H_c B_c}{D_e^2}\right)\left[\frac{(H_c + S_c/D_c)}{(L_c + Z_c/D_c)(L_{cs}/D_c)(J_c/D_c)}\right]^{1/3}$

A comparative assessment of these empirical relations showed a wide-spread among the estimated pressure-drop values and is presented in section 4.4. In practice, this value is to be apriori estimated for allowing in-situ operation of this device with solar thermal system. Pressure-drop also depends on temperature in lieu of fluid property for a given mass flow rate, [Gimbun *et al.*, 2004]. Generally, Lapple-type model is employed with various coefficients. However, it can be inferred that some of these models are independent of geometry (height/diameter) of the cyclone separator. This is not obvious, as pressure-drop is expected to vary with diameter of cyclone or height. In view of such observations, experiment and detailed computational fluid dynamics (CFD) analysis is performed. This is presented in the next section.

4.3 EVALUATION OF A CYCLONE SEPARATOR

In this section experiment and CFD analyses are performed for evaluation of the designed cyclone separator. These are presented subsequently.

4.3.1 Experiment: Pressure-drop

As explained, the pressure-drop across inlet and outlet in cyclone separators is required for estimating the power requirement for operating this device. To obtain the same, the experiments are performed with a cyclone separator having dimensions as in Figure 4.1. The parameters are selected based on a preliminary analysis to achieve the desired collection

efficiency > 95% for a particle size ≤ 50 μm. The experiments are performed with an area-averaged inlet air-speed of up to 15 m/s that are measured with the hot-wire anemometer (make: Fisher Scientific (06-662-73)) at room temperature (~ 30-35 °C) with accuracy of ~ ±1 %. Pressure-drop between the inlet and outlet of cyclone separator is measured with the differential pressure transducer of Dwyer 475-0-FM make for up to 2490 Pa, resolution ~2.5 Pa and accuracy ~ ±1.5 %. An overall uncertainty of about 10% is associated to account for the observed variability during pressure and average speed measurements. The schematic of experimental system is given in Figure 4.3.

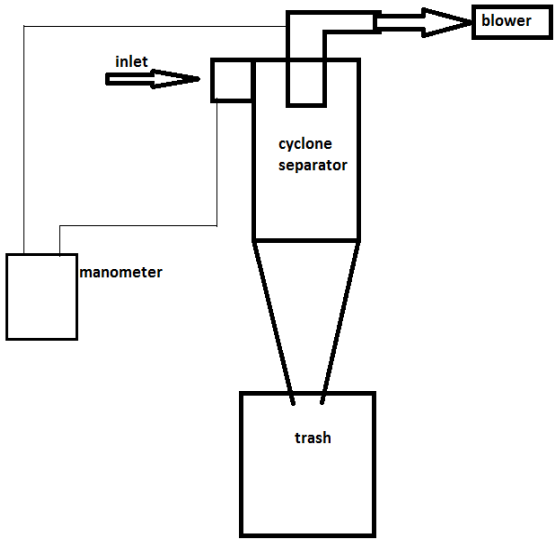

Figure 4.3: Schematic of experimental set-up for pressure-drop measurement.

4.3.2 Numerical Analysis

For the analyses of 2D2D cyclone separator, as in Figure 4.1, ANSYS Fluent 13.0 is employed. Conservation of mass and momentum equations are solved for analyzing the flow in a cyclone separator at the steady-state. The area-averaged air speed of 4-16 m/s at the inlet and zero gauge pressure (atmospheric pressure) at the outlet are the prescribed boundary conditions. All the walls are treated as no-slip, as usual.

Table 4.3: Numerical set-up for CFD analysis.

Mesh	Resolution (in mm)	Boundary layer	Equations	Numerical scheme	Convergence
Polyhedral	2, 3, 4	Y+ ~ <5 Growth factor ~ 1.2	Continuity, Momentum	2^{nd} order upwind	10^{-5} - 10^{-6}

The adopted numerical set-up is presented in Table 4.3. This table also presents the resolution of employed polyhedral mesh, ranging from 2 mm to 4 mm. The mesh resolves boundary layer near the wall that is necessary for an acceptable prediction of the velocity profiles in the considered cyclone separator design.

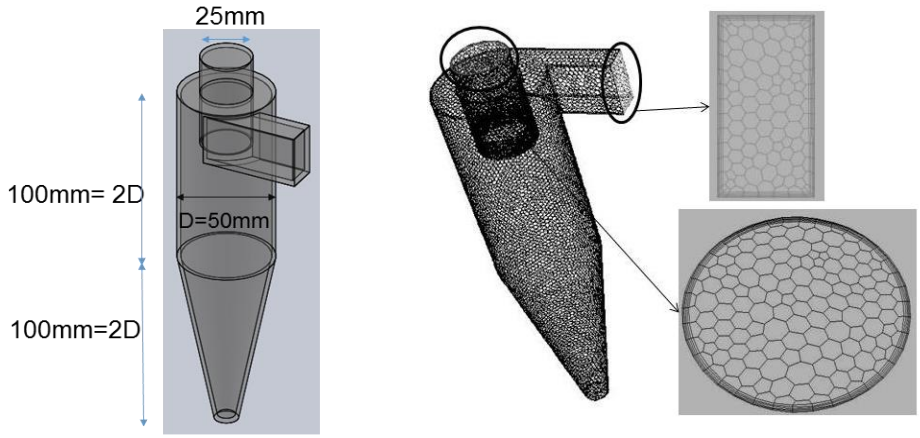

a. Modeled cyclone separator

b. Generated mesh

Figure 4.4: The modeled cyclone separator and an example of generated mesh for CFD analysis.

The employed convergence criteria maintain the minimum quality of CFD analyzed results. The modeled cyclone separator geometry with dimension is shown in Figure 4.4(a) as an example. The employed polyhedral mesh with the wall resolved boundary layer is also presented in Figure 4.4(b).

4.4 RESULTS AND DISCUSSION

4.4.1 Validation

A comparison between the experiment, the empirical models predicted and the CFD analyzed pressure-drop between the inlet and outlet of the cyclone separator is presented in Figure 4.5.

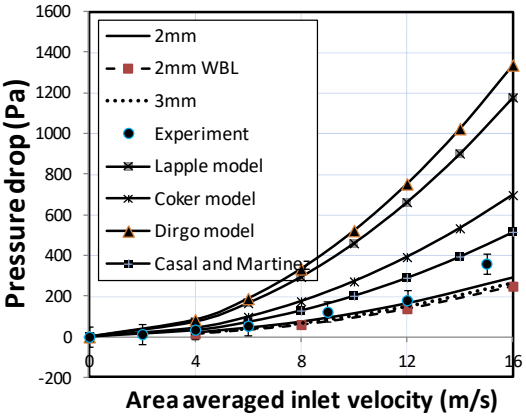

Figure 4.5: Comparison of CFD and experimental pressure-drop.

Variations of about 10-15% between experimentally measured and CFD analyzed pressure-drop are observed. This is much lower than that of variability between the well-known correlations and the resulting uncertainty. It is to be noted that all these models are derived from Lapple model using various pressure-drop coefficients, see Table 4.2. Therefore, an improvement in this model by including the geometry effect is expected to provide the desired correlation. This validation provides confidence on the performed experiment and the adopted CFD set-up. This also reveals that for the considered design and experimental conditions the laminar approach is sufficient.

4.4.2 Physics of Dust Removal

The CFD analyzed velocity profiles for an area-averaged inlet air speed of 12 m/s are presented in Figure 4.6. The different radial lines (section 1-1-, 2-2 and 3-3) along the height (y-direction) at which these profiles are plotted are shown in Figure 4.6(a). The inlet and outlet of the cyclone separators are depicted by arrows. From this figure following can be inferred:

a. The CFD analyzed vertical (y) velocity profiles are compared for different mesh resolution, namely, 2-4 mm. Based on this comparison (Figure 4.6(b)), for further investigation a mesh resolution of about 2-3 mm is preferred.
b. The positive values of vertical (y) velocity component at the center region, which is away from boundary, depict the effect of suction at the outlet, when applied (see Figure 4.6(a)). This can be inferred from its increasing values towards the outlet, as indicated by various sections, 1-1, 2-2 and 3-3 in Figure 4.6(a).
c. The negative values of vertical (y) velocity at the near-wall region are attributed to the downward movement of air along the helical path as shown in Figure 4.6(c). The CFD analyzed vertical velocity profile clearly demonstrates that the near-wall region is captured using the employed wall resolved mesh. Such a mesh is, therefore, recommended for future investigation (Figure 4.4).

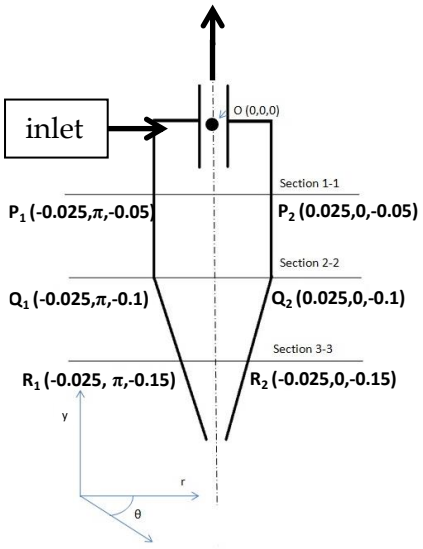

a. Analyzed sections in cyclone separator

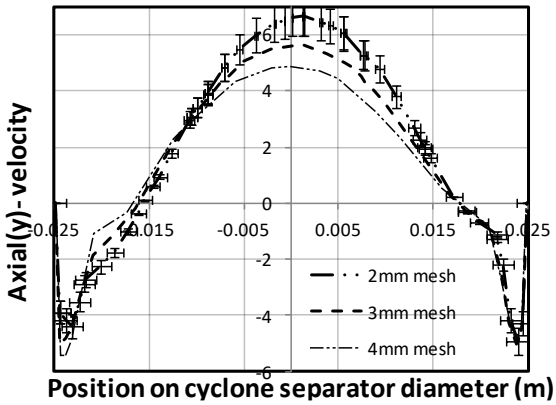

b. Vertical velocity profile for grid dependence, section 1-1

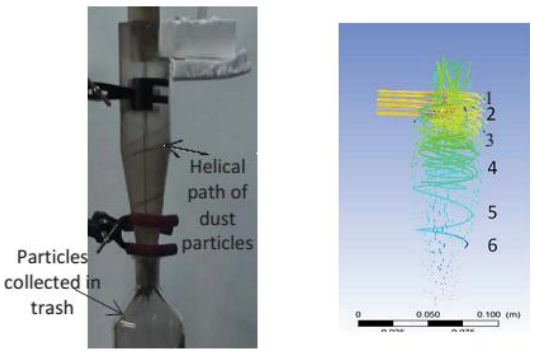

c. Helical path of dust and streamlines of air flow in cyclone separator[15]

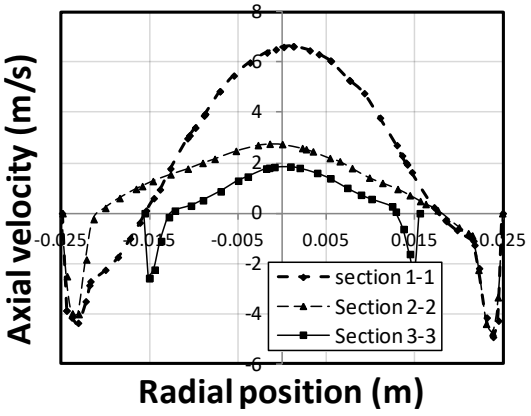

d. Vertical velocity profile along height (y-direction)

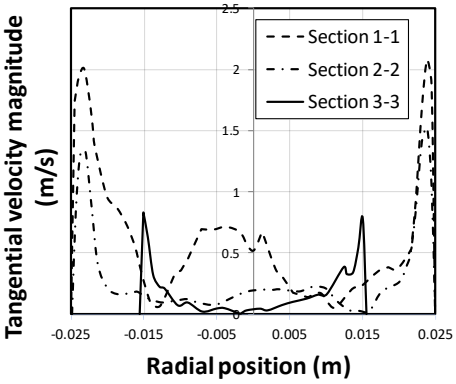

e. Tangential velocity at different sections

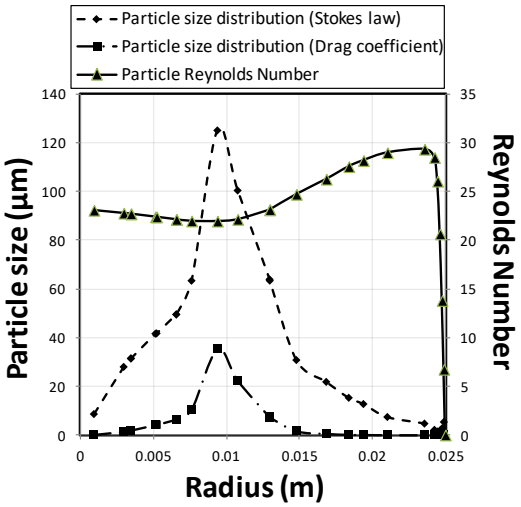

f. Particle size and Particle Reynolds number distribution

Figure 4.6: Velocities at different sections of cyclone separator and helical streamlines of air.

d. The values of vertical velocity magnitude decrease towards the conical region as a result of enhanced friction effect. Thus, the generated vortex in barrel eventually dissipates in the conical region. The vertical (y) velocity magnitude then increases in inner vortex towards outlet. This is also shown in the CFD analyzed helical streamlines (Figure 4.6(c)). Obviously, the highest velocity magnitude is expected at the inlet to the cyclone separator.

e. Figure 4.6(e) shows the tangential velocity at various sections of cyclone separator. The magnitude of the tangential velocity increases, nearly, linearly near the wall region (say, $0.02 \leq r$ (m) ≤ 0.025). This indicates the presence of forced vortex in this region, which is consistent with the inferred viscous effect near the wall as observed in Figure 4.6(d).

f. Tangential velocity decreases, along radial direction, away from the wall, which denotes the presence of free vortex region (say, $0.015 \leq r$ (m) < 0.02). In this region, viscous effects are negligible. In the cyclone separator for $0.0 \leq r$ (m) < 0.015, the type of vortex cannot be predicted from Figure 4.6(e).

g. Figure 4.6(f) shows the calculated particle size distribution at the section 1-1 using CFD analyzed velocity profiles. These are obtained using eqs. (4.8) and (4.11). In this figure $r = 0$ indicates the centre and $r = 0.025$ indicates the wall of designed cyclone separator. This analysis shows that small particles, say < 20 µm, will leave the cyclone separator near the centre as a result of high vertical velocity. The larger sized particles are expected to move towards the wall as a result of centrifugal force and to separate as a result of helical flow streamlines.

h. Particle Reynolds number is given by $Re_{d_p} = \rho_f v d_p / \mu$, where d_p is diameter of particle. Radial variation of particle Reynolds number (50 µm diameter) at the section 1-1 is shown in Figure 4.6(f). This clearly illustrates that the Stokes law is valid only in the boundary layer near the wall. Thus, the drag force based formulation will be valid in most of the region. Thus, the particles size, say, >10 µm, will be collected near the wall.

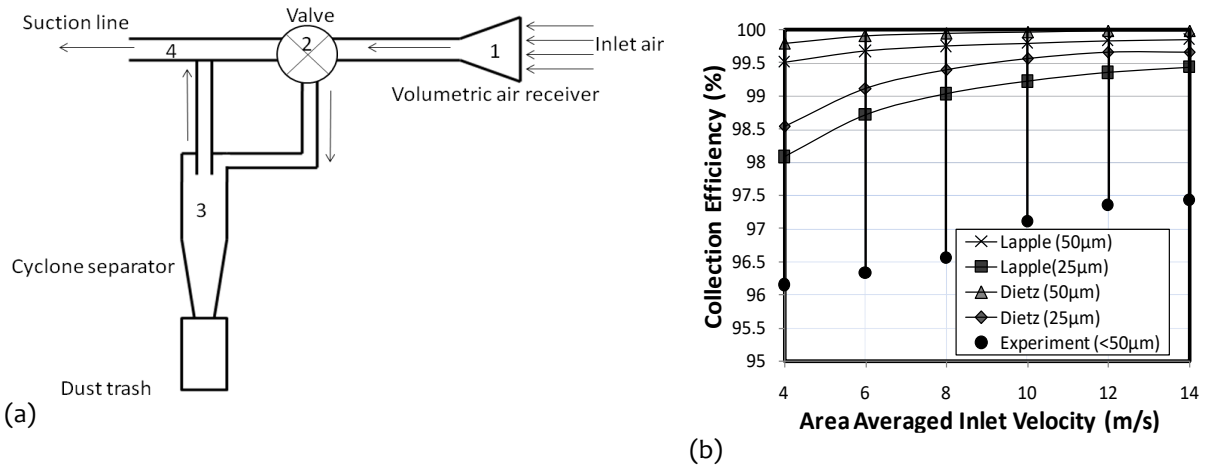

Figure 4.7: (a) A strategy for cleaning of porous absorber based OVAR and (b) experimental evaluation of collection efficiency for the designed cyclone separator.

Figure 4.7(a) shows a strategy, which can be adopted for cleaning of porous absorber during its operation. Following practical aspects are to be considered for its installation:

a) avoid interference with the concentrated solar irradiance onto the absorbers;
b) prevent the transport of dust to the internals of central receiver system;
c) in-situ operation with the receiver or on demand and its periodical cleaning during off-hours.

Also, in view of dust collection the designed cyclone separator (see Figure 4.1) is experimentally evaluated, see e.g. [Singh, 2014]. For completeness, the experimental results are presented in Figure 4.7(b). This clearly demonstrates that the collection efficiency increases with inlet area averaged air-speed. Furthermore, the collection efficiency, as expected, is higher for larger particle sizes. These obtained experimental values with particle sizes of < 50 μm are compared with the experimental correlations by Lapple (1951) and Dietz (1981). Thus, it is inferred that such models are applicable for practical applications of cyclone separator during cleaning operation of OVAR. However, higher inlet air-speed indicates higher pressure-drop. This may limit the application of such a cleaning device. Therefore, for practical utility, it is necessary to estimate the pressure-drop by using a simplified correlation. This is presented in the subsequent sub-sections.

4.4.3 Pressure-drop Coefficient

As already explained, geometrical aspects are to be included in estimation of pressure-drop, may be, in the form of a simple coefficient. To obtain such a parameter, cyclone separator geometries 1-7 are analyzed using the validated CFD tool. All these geometries are 2D2D type. In these geometries the cyclone diameter is varied between 25-175 mm. These are summarized in Table 4.4.

Table 4.4: Different employed geometries for CFD analysis.

Geometry	**1**	**2**	**3**	**4**	**5**	**6**	**7**
Diameter (mm)	25	50	75	100	125	150	175

The presented well-known pressure-drop correlations in Table 4.2, in principle, follows Lapple-type model. In this model K is taken as constant value of 16. In the model by Coker (1993), the value of K is fixed at 9.47. Considering this, the following systematic approach is adopted for estimation of the coefficient K:

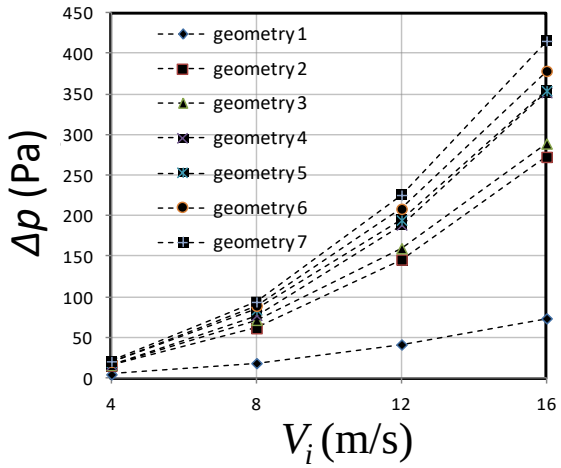

Figure 4.8: Pressure-drop in various geometries of 2D2D cyclone separators at different velocities.

Step 1: Using the adopted CFD numerical set-up the pressure-drop for these considered geometries (1-7) are calculated. The pressure-drop of a given geometry is plotted with respect to the area-averaged inlet air-speed of air in Figure 4.8. This shows that the pressure-drop increase with air-speed as well as the diameter of cyclone separator for a given inlet velocity.

Step 2: Investigation of the CFD analyzed values of the coefficient *K*, in comparison with Lapple model, in general, revealed its logarithmic nature, which is as follows:

$$K = C_1 \ln V_i + C_2 \ . \tag{4.12}$$

Where C_1 and C_2 are coefficients and V_i is the area averaged inlet air-speed. Further evaluation reveals that the value of C_1 depends on cyclone diameter in an exponential form, which is estimated as:

$$C_1 = 0.106e^{0.013D_c} \ . \tag{4.13}$$

Step 3: Value of C_2 is estimated as an average value for the considered geometries 1 to 7. Combining all these, the following logarithmic profile for *K* is obtained:

$$K = 0.106e^{0.013D_c} \ln V_i + 3.4 \tag{4.14}$$

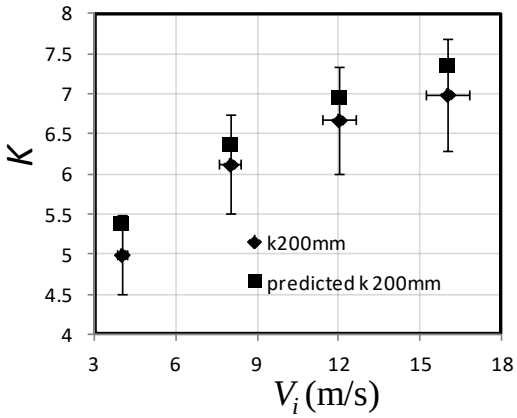

Figure 4.9: A comparison between CFD and predicted K values for 2D2D cyclone separator of 200 mm diameter.

The developed coefficient, thus, includes the effect of geometry in the widely employed Lapple type models. In order to test the applicability or predictive capability of this logarithmic approximation, a 2D2D cyclone separator design with a diameter of 200 mm is considered. This geometry is not considered in obtaining the logarithmic profile of *K*. The pressure-drop in this geometry is calculated using the adopted CFD approach. The predicted values of *K* using the

presented logarithmic model is compared to that of CFD analyzed values of *K* for different inlet velocities. The comparison is presented in Figure 4.9. This shows that the CFD analyzed (denoted by k200mm) and the derived logarithmic profile (denoted by predicted k200mm) compares within 10%. Therefore, it can be inferred that using the logarithmic approximation of *K* in Lapple model instead of a constant value will lead to improvement in pressure-drop estimation.

4.4.4 Effect of Air Temperature on Pressure-drop

In addition, the thermo-physical properties of air depend on temperature. Therefore, the influence of operating temperature is to be included in the estimated pressure-drop coefficient as well. For instance, density of air decreases and its absolute viscosity increases with temperature. To combine the effect of temperature on kinematic viscosity that affects pressure-drop, is analyzed by adapting the property ratio method [Schlichting and Gersten, 2004]. Here, the pressure-drop is related to ratio of kinematic viscosity with respect to a reference temperature as:

$$\Delta p/\Delta p_\infty = (\nu/\nu_\infty)^c \tag{4.15}$$

The subscript ∞ denotes the property at reference ambient temperature of 30°C. For pressure-drop coefficient *K*, the pressure-drop relation can be expanded such that:

$$K\rho/K_\infty\rho_\infty = (\nu/\nu_\infty)^c \tag{4.16}$$

$$\therefore K/K_\infty = \frac{(\nu/\nu_\infty)^c}{(\rho/\rho_\infty)} \tag{4.17}$$

The CFD simulations with the validated and adapted approach are performed for a temperature range of 300 K-1100 K with variable air properties to calculate pressure-drop. This range includes the over-all operating condition of open volumetric air receiver based system [Hoffschmidt *et al.*, 2003; Ávila-Marín 2011]. The Figure 4.10(a) shows that the pressure-drop increases with temperature for a given inlet Reynolds number ($Re_{d_h} = \rho_f v d_h/\mu$) where d_h is hydraulic diameter of cyclone separator inlet. Thus, it is inferred that in-situ operation of such a cleaning device at higher temperature needs special attention as the pressure-drop directly affects the over-all system performance. Therefore, it is advisable that such a cleaning device, preferably, be operated only during extreme condition.

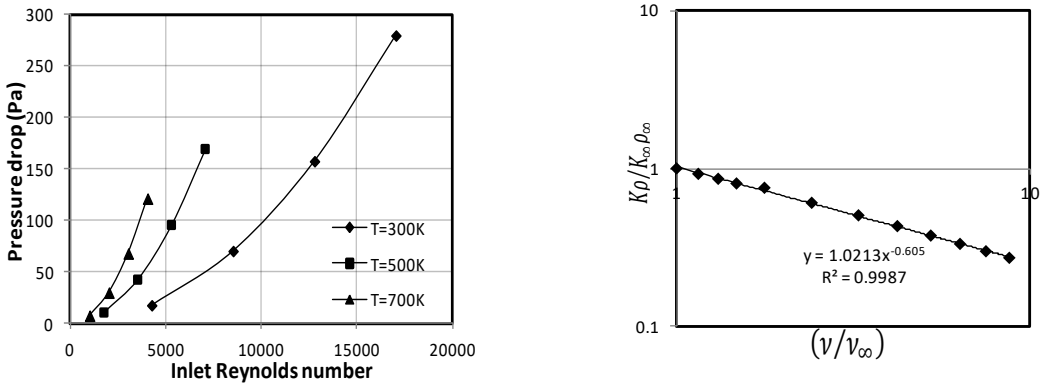

a)Pressure-drop variation with inlet Reynolds number *b)Plot of property ratio method (logarithmic scale)*

Figure 4.10: Effect of temperature on pressure-drop.

Figure 4.10(b) reveals that K-factor depends on kinematic viscosity (corresponding temperature) as:

$$K/K_{\infty} = 1.0213 \frac{(\nu/\nu_{\infty})^{-0.605}}{(\rho/\rho_{\infty})}. \quad (4.18)$$

This results in the following modified approximation of K-factor based on reference temperature as:

$$K = 1.0213 \frac{(\nu/\nu_{\infty})^{-0.605}(0.106e^{0.013D_c} \ln V_i + 3.4)}{(\rho/\rho_{\infty})}. \quad (4.19)$$

The open volumetric air receiver can be operated at a temperature as high as 1000 °C as already explained in Chapter 1. Thus, for evaluating the applicability of modified K-factor approximation as in eq. (4.19) the obtained pressure-drop values are compared with CFD analyzed values as shown Figure 4.11 for temperature of up-to 1250 K. For this comparison an inlet Reynolds number of ~12700 is maintained. As already observed, an uncertainty of ± 10% is associated with CFD analyzed values. Thus, it inferred from Figure 4.11 that the derived modified *K*-factor approximation provides acceptable prediction of pressure-drop.

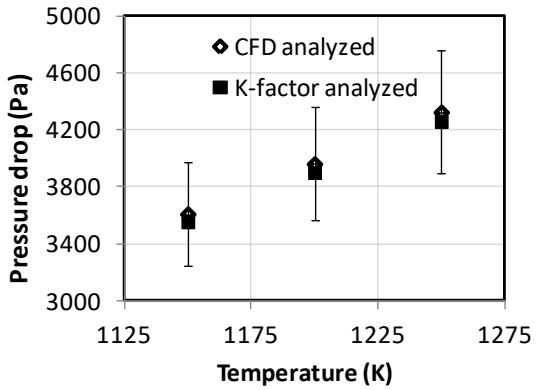

Figure 4.11: Comparison between CFD analyzed and K-factor based pressure-drop.

4.5 SUMMARY

In this chapter design and evaluation of cyclone separator, which is required for cleaning and collection of dust for open volumetric air receiver is presented. This is necessary for operating an open volumetric air receiver based concentrated solar thermal system in arid desert regions, like, Rajasthan. The design of cyclone separator is based on the desired efficiency for a particle size with a given air mass flow rate. The operation of this system will depend on the required power or equivalently, on the pressure-drop across the designed cyclone separator. Experiments and the steady-state computational fluid dynamics analysis are presented. The comparison between measured and computed pressure-drop reveals that the adopted numerical approach for CFD analyses is acceptable. Furthermore, the numerically obtained velocity profiles reveal the formation of helical air flow streamlines. The analysis of computed vertical velocity profiles provides further insight to the flow and removal of dust in the cyclone separator. Finally, using the validated and adopted numerical set-up a logarithmic model for the coefficient in pressure-drop correlation as in widely used Lapple model is derived. The pressure-drop coefficient is further generalized including temperature effects using property ratio method. Consequently, a realistic estimation of power requirement for operating such a device would allow justifying its operation, say, at all time or during a particular event, such as, dust storm.

Although, cyclone separator may serve the purpose of mitigating dust deposition, however its operation will require extra power at the blower. Hence, an analysis to derive a suitable operating condition to operate an open volumetric air receiver with cyclone separator is presented in the next chapter.

…